

# 中国激光

## 激光刻蚀对 Ag/FTO/AZO 薄膜光学 和电学性能的影响

周运龙<sup>1</sup>, 雷敏<sup>1</sup>, 王陈林<sup>1</sup>, 许倩<sup>1</sup>, 李保家<sup>1,2\*</sup>, 黄立静<sup>2,3\*\*</sup>

<sup>1</sup> 江苏大学材料科学与工程学院, 江苏 镇江 212013;

<sup>2</sup> 江苏大学微纳光电子与太赫兹技术研究院, 江苏 镇江 212013;

<sup>3</sup> 江苏大学机械工程学院, 江苏 镇江 212013

**摘要** 采用不同能量密度的激光对制备的 Ag/FTO/AZO 多层薄膜进行光栅结构刻蚀, 分析激光刻蚀后薄膜的表面形貌、光学性能和电学性能的变化, 并确定薄膜获得最佳性能时的激光能量密度。结果表明, 以一定的激光能量密度对薄膜进行光栅结构刻蚀处理, 不仅能有效提高薄膜的抗反射能力, 还能产生附加退火作用, 促使薄膜晶粒生长, 减少晶界面积, 从而减少晶界的光子和载流子的散射损失, 提高载流子的迁移率, 最终提高薄膜的透过率, 优化薄膜的导电性能, 实现薄膜的光学性能和电学性能的优化。

**关键词** 激光加工; Ag/FTO/AZO 薄膜; 光栅结构; 光学性能; 电学性能

中图分类号 V261.8; O484.4; TB34 文献标志码 A

doi: 10.3788/CJL202249.0202007

### 1 引言

在太阳能电池、液晶显示器等光电器件领域, 具有高透光性和低电阻率的透明导电氧化物(TCO)薄膜是应用最广泛的功能材料之一<sup>[1-2]</sup>。而在常见的 TCO 薄膜中, 掺铝氧化锌(AZO)薄膜有着原材料丰富、化学/热稳定性高、成本低、无毒等优点, 因此具有良好的应用前景<sup>[3]</sup>。此外, 通过复合不同性质的薄膜可以改善单层薄膜的某些性能, 因而多层薄膜也成为当前的研究热点<sup>[4]</sup>。李明亮等<sup>[5]</sup>发现, 在 AZO 薄膜表面复合一定厚度的金属 Ag 层可以显著提高薄膜的导电性。但是, 在 Ag 层与 AZO 薄膜复合时, 不可避免地会出现薄膜的光反射损失, 导致薄膜透光性变差。有学者研究发现, 将掺氟二氧化锡(FTO)层与 AZO 层复合, 得到的多层薄膜的抗还原能力优于单层 AZO 或 FTO 薄膜, 多层薄膜的稳定性明显增强<sup>[6]</sup>; 而且将 FTO 层与 Ag 层和 AZO 薄膜进行复合, 还可以在一定程度上抑制薄膜的光反射<sup>[7]</sup>。需要指出的是, FTO 层对薄膜中光反射的抑制作用很有限, 且 FTO 层过厚也会导致薄

膜的透光性下降。因此, 进一步采取其他有效措施来减少薄膜的光反射损失是一个值得深入研究的课题。

在薄膜表面引入特定的微纳结构可以起到很好的抗反射作用, 而光栅结构就是常用的抗反射微纳结构之一<sup>[8-10]</sup>。在薄膜表面制备光栅结构的方法主要有激光刻蚀法<sup>[11-13]</sup>、电子束光刻法<sup>[14]</sup>、等离子刻蚀法<sup>[15-16]</sup>和纳米压印法<sup>[17-18]</sup>。但电子束光刻法、等离子刻蚀法和纳米压印法具有工艺复杂、制备周期长且成本相对高等缺点, 而 Yamada 等<sup>[19]</sup>的研究表明激光刻蚀能够更快速地在金属玻璃表面制备出光栅结构, 而且成本更低。2019 年 Canteli 等<sup>[20]</sup>在 AZO 薄膜表面利用激光刻蚀出相互平行和相互垂直的两种光栅结构, 发现以这些薄膜样品为电极的太阳能电池的光散射效应较弱, 但短路电流增大。最近本课题组也开展了单层 AZO 薄膜表面激光刻蚀抗反射光栅结构的研究, 结果表明激光刻蚀后的 AZO 薄膜综合性能明显提高<sup>[21]</sup>。值得一提的是, 在激光刻蚀薄膜的过程中, 会产生附加激光退火作用, 促进薄膜的再结晶和晶粒生长, 从而改善薄膜的

收稿日期: 2021-05-26; 修回日期: 2021-06-20; 录用日期: 2021-07-08

基金项目: 国家自然科学基金(51805220, 61405078)、江苏大学科研课题立项资助(19A003)

通信作者: \*li\_bjia@126.com; \*\*lij\_huang@126.com

光学性能和电学性能<sup>[22]</sup>。因此,本文使用 532 nm 波长的纳秒脉冲激光在不同激光能量密度下对由磁控溅射法制备得到的 Ag/FTO/AZO 薄膜进行光栅结构刻蚀处理,再对刻蚀处理后的薄膜进行表面形貌和性能分析,着重研究激光能量密度对薄膜透光性能和导电性能的影响,从而确定实现 Ag/FTO/AZO 薄膜性能优化的最佳激光能量密度。此研究结果可为多层透明导电薄膜的性能优化提供一定的参考,也可为激光刻蚀光栅结构的应用提供科学依据。

## 2 实验

### 2.1 Ag/FTO/AZO 多层薄膜的制备

首先将商售的 AZO 薄膜/玻璃(15 mm×15 mm, AZO 层厚度为 750 nm)依次放入盛有去离子水、丙酮溶液和无水乙醇溶液的玻璃器皿中超声清洗 10 min, 将清洗好的样品用高纯氮气吹干, 待冷却后将薄膜样品放好备用。

将处理好的 AZO 薄膜/玻璃基底放置在射频磁控溅射仪(VTC-2RF, 合肥科晶材料技术有限公司, 中国)的样品台上, 将纯度为 99.999% 的 FTO 和纯度为 99.99% 的 Ag 圆片作为靶材依次溅射, 以制备 Ag/FTO/AZO 多层薄膜。溅射条件是在溅射室本底真空度达到 4 Pa 后充入高纯氩气, 之后控制工作压强为 15 Pa, 功率为 60 W, 最后由在线测控仪控制膜厚, 保持 FTO 层和 Ag 层厚度分别为 10 nm 和 5 nm。

### 2.2 Ag/FTO/AZO 多层薄膜的激光刻蚀处理

将制备好的 Ag/FTO/AZO 多层薄膜样品放置在二极管泵浦 Nd:YVO<sub>4</sub> 纳秒脉冲激光系统

(Wedge 532, Bright Solutions 公司, 意大利)的移动样品台上, 扫描路径为 X 方向单向逐线扫描, 扫描区域为 10 mm×10 mm。在扫描速度为 10 mm/s、离焦量为 0.5 mm(焦前)、线间距为 0.1 mm 的条件下, 分别采用 0.1, 0.3, 0.7, 1.3, 2.1 J/cm<sup>2</sup> 的激光能量密度( $D_{ener}$ )对所制备的多个 Ag/FTO/AZO 薄膜样品表面进行光栅结构刻蚀处理。在激光刻蚀处理完成之后, 取出薄膜样品, 通过洗耳球轻吹, 将薄膜样品表面的飞沫去除干净。

### 2.3 表征与测试

将激光刻蚀后的薄膜样品用扫描电子显微镜(SEM; S-3400N, Hitachi 公司, 日本)观察表面形貌, 再通过共聚焦激光扫描显微镜(CLSM; VK-X250, Keyence 公司, 日本)测量激光刻蚀光栅结构的高度, 利用 X 射线衍射仪(XRD; D8 Advance, Bruker 公司, 德国)检测薄膜样品的晶体结构。薄膜样品的透过率和反射率由紫外-可见分光光度计(UV-8000, 上海元析仪器有限公司, 中国)测量, 薄膜样品的方块电阻由数字式四探针测试仪(RTS-9, 广州四探针科技有限公司, 中国)测出。

## 3 分析与讨论

### 3.1 表面形貌分析

图 1 为 AZO 薄膜和 Ag/FTO/AZO 多层薄膜的 SEM 图。从图 1(a)可以看到, 单层 AZO 薄膜表面分布着较小的 AZO 粒子, 表面起伏不明显。从图 1(b)可以看到, 在镀上 FTO 层和 Ag 层后, 薄膜表面的形貌并没有发生明显的变化, 这可能是因为溅射所镀的 Ag 层和 FTO 层的膜厚较小, 从而对薄膜表面形貌的影响也很小<sup>[23]</sup>。

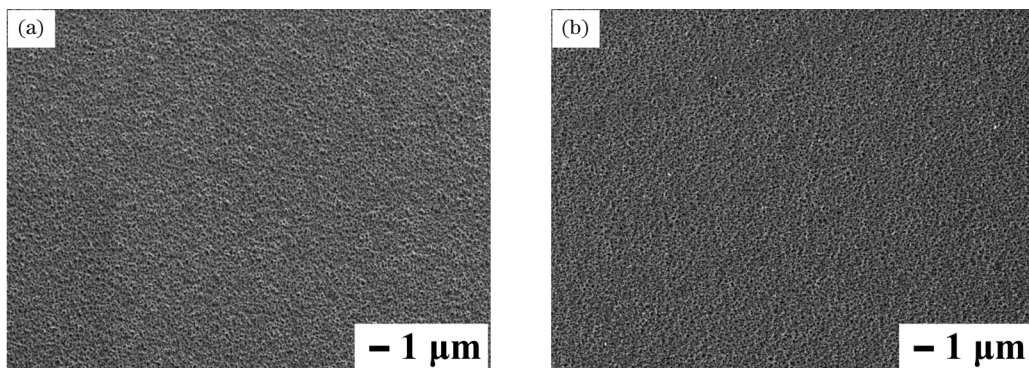


图 1 薄膜的 SEM 图。(a) AZO 薄膜;(b) 原始 Ag/FTO/AZO 多层薄膜

Fig. 1 SEM images of thin films. (a) AZO film; (b) as-prepared Ag/FTO/AZO multilayer film

图 2 所示为不同能量密度下激光刻蚀处理后 Ag/FTO/AZO 多层薄膜的表面形貌。可以看出, 激光刻蚀后的薄膜表面有着明显可见的光栅结

构, 其中同一幅图内较明亮的条状区域是未处理的薄膜层, 较暗的区域则是激光刻蚀产生的凹槽。图 3 所示为不同能量密度下 Ag/FTO/AZO 薄膜

表面激光刻蚀光栅结构的高度。可以看到,随着激光能量密度的增大,光栅结构高度也在不断地增加且光栅结构高度都超过了镀上的Ag层和FTO层的总厚度(15 nm)。当激光能量密度为0.1 J/cm<sup>2</sup>时,如图2(a)所示,多层薄膜刻蚀光栅凹槽的边缘不平整且存在类似毛刺的材料残余区域,此现象在文献[7]中也有报道,且结合图3可以发现,此时刻蚀光栅结构的高度仅为95 nm。产生这种现象的原因可能是激光刻蚀的能量密度过小,只能在薄膜表面刻蚀出较浅的深度,且不能够在刻蚀的过程中将刻蚀区域全部熔融。随着能量密度从0.3 J/cm<sup>2</sup>增加到1.3 J/cm<sup>2</sup>,如图2(b)~(d)所示

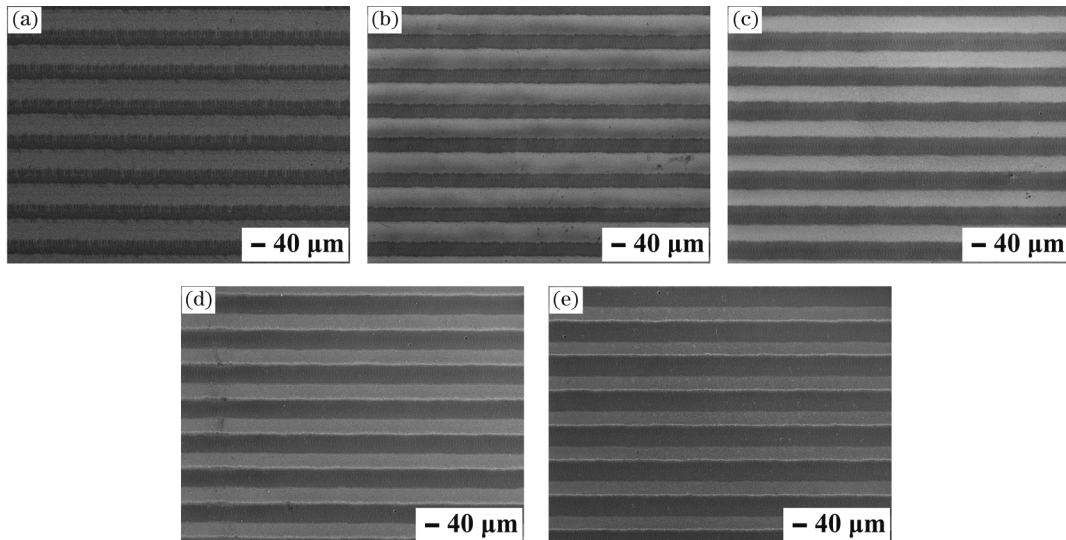


图2 不同能量密度下Ag/FTO/AZO多层薄膜的SEM图。(a) 0.1 J/cm<sup>2</sup>; (b) 0.3 J/cm<sup>2</sup>; (c) 0.7 J/cm<sup>2</sup>; (d) 1.3 J/cm<sup>2</sup>; (e) 2.1 J/cm<sup>2</sup>

Fig. 2 SEM images of Ag/FTO/AZO multilayer films under different laser energy densities. (a) 0.1 J/cm<sup>2</sup>; (b) 0.3 J/cm<sup>2</sup>; (c) 0.7 J/cm<sup>2</sup>; (d) 1.3 J/cm<sup>2</sup>; (e) 2.1 J/cm<sup>2</sup>

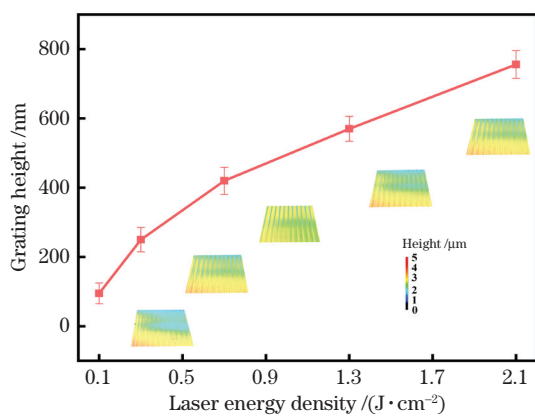


图3 不同能量密度下Ag/FTO/AZO多层薄膜表面激光刻蚀光栅结构的高度

Fig. 3 Heights of laser-etched grating structures on Ag/FTO/AZO multilayer films under different laser energy densities

示,多层薄膜刻蚀凹槽的边界逐渐变得整齐规则,且类似毛刺的区域逐步消失,同时凹槽的宽度逐渐增大,这是因为随着激光能量密度的增加,薄膜刻蚀区域产生Marangoni对流现象,并与温度差、压力差共同推动熔融的薄膜层材料,促使熔化的薄膜材料向低温区域扩展,进而增加了刻蚀凹槽的宽度和深度<sup>[24-25]</sup>。当能量密度为0.7 J/cm<sup>2</sup>时,薄膜达到了最佳的刻蚀效果,这是因为此时的能量密度较为合适,在将刻蚀区域的薄膜熔化的同时也不会产生过大的温度差和压力差,从而不会过分烧蚀凹槽两边区域,所以能够产生边界分明的刻蚀凹槽。当激光能量密度增加到2.1 J/cm<sup>2</sup>时,如图2(e)所示,薄膜

刻蚀凹槽表面除了槽宽继续变大外,没有其他明显的变化,但是根据图3,此时刻蚀光栅结构的高度为756 nm,近乎刻蚀到玻璃基底了,这应该是激光能量密度过大造成的。

### 3.2 XRD分析

图4所示为不同能量密度下薄膜的XRD图谱,可以看到,薄膜图谱都显示出对应于ZnO六方纤锌矿结构的(002)特征峰,说明薄膜都具有沿(002)面择优生长的趋势。另外,在AZO薄膜表面镀上的Ag层和FTO层非常薄,以致于图4所示的所有图谱均未显示出对应于Ag和FTO的特征峰,这与文献[26-27]的相关描述类似。从图4可以看出,随着能量密度从0.1 J/cm<sup>2</sup>增加到0.7 J/cm<sup>2</sup>,Ag/FTO/AZO薄膜的ZnO(002)的半峰全宽(FWHM)逐渐变窄,表明激光刻蚀过程中产生的附

加退火作用会促进薄膜的晶粒生长,减少晶体缺陷,使薄膜的结晶度得到了提高<sup>[28]</sup>。当能量密度增加到1.3 J/cm<sup>2</sup>和2.1 J/cm<sup>2</sup>时,此时的衍射峰强度明显减小,主要原因可能是随着激光能量密度的增大,单位面积上积聚的热量增多,导致晶格的无序性增强<sup>[26]</sup>,从而降低了衍射峰的强度。由此可以看出,选用合适的激光能量密度进行光栅结构刻蚀,其产生的附加退火作用能够对薄膜的晶体结构起到一定的改善作用。

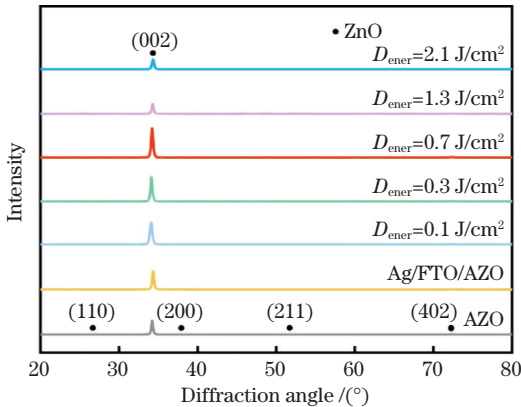


图4 不同薄膜的XRD图谱

Fig. 4 XRD patterns of different films

### 3.3 光学性能分析

图5所示为不同能量密度下薄膜的透射光谱。可以看出,与原始AZO薄膜相比,未处理的Ag/FTO/AZO多层薄膜的透过率明显较低,这是因为AZO表面覆盖了FTO层和Ag层。相对于未处理的Ag/FTO/AZO多层薄膜,激光刻蚀过的薄膜透过率明显增大,这是因为通过激光刻蚀制备的光栅结构具有一定的抗反射能力<sup>[21]</sup>,同时在刻蚀过程中产生的附加激光退火促进了薄膜中晶粒的生长且减少了晶体的缺陷数量,使得晶界和晶体缺陷处的光散射损失减少。图6所示为不同薄膜在400~800 nm波段的平均透过率。从图6可以直观地看出,当能量密度从0.1 J/cm<sup>2</sup>增加到0.7 J/cm<sup>2</sup>时,薄膜的透过率持续增大,原因包括:1)随着激光能量密度的增加,刻蚀光栅结构凹槽的宽度增大(图2),薄膜减薄的区域变大,有利于提高薄膜的透过率;2)光栅结构高度虽然随着激光能量密度的增大而增加,但是高度也不太大(图3),因此光栅结构的侧面面积增大,且光在光栅外表面的反射损失减少,从而提高了薄膜的抗反射能力<sup>[21]</sup>;3)结合XRD图谱分析,刻蚀产生的附加激光退火作用使薄膜中的晶粒长大,晶体缺陷数量减少,从而有效减少薄膜中的光散射损失<sup>[29-30]</sup>。当激光能量密度为0.7 J/cm<sup>2</sup>时,薄膜表

面光栅结构的高度和凹槽宽度适中,此时薄膜表面起到了较强的抗反射作用,同时激光刻蚀过程中产生了较强的附加退火作用,因此薄膜的平均透过率达到最大值。当能量密度为1.3 J/cm<sup>2</sup>时,薄膜的透过率明显降低,这是因为光栅结构的高度过大,抑制了薄膜的抗反射能力,且过大的能量密度造成晶格的无序性增强。关于光栅结构的抗反射作用将通过反射光谱测试结果进一步讨论。当能量密度继续增加到2.1 J/cm<sup>2</sup>时,由于能量密度太大,激光刻蚀的深度(即光栅结构的高度)过大,刻蚀到了玻璃基底,使得入射光可经凹槽直接透射,因此透过率反而升高。

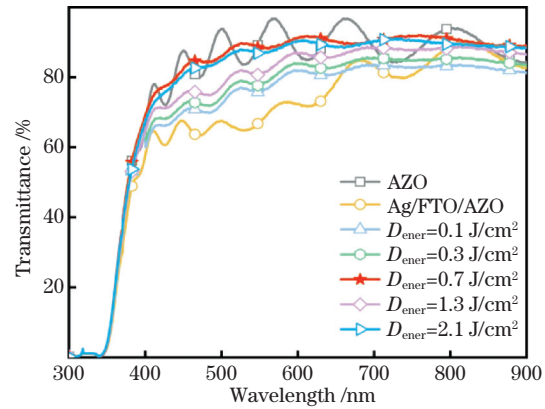


图5 不同薄膜的透射光谱

Fig. 5 Transmittance spectra of different films

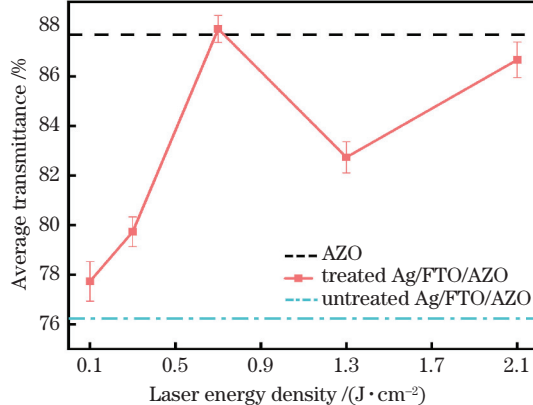


图6 不同薄膜的平均透过率(400~800 nm)

Fig. 6 Average transmittance values (400~800 nm) of different films

图7所示为不同能量密度下薄膜的反射光谱,可以看到,未处理的Ag/FTO/AZO多层薄膜的反射率明显低于原始AZO薄膜,这可能是因为原始AZO薄膜表面较为平坦,对入射光产生了一定的镜面反射,而FTO层的加入有效抑制了薄膜内的光反射<sup>[7]</sup>。与未处理的Ag/FTO/AZO多层薄膜的反射率相比,经过激光刻蚀的薄膜的反射率在其上下

波动。图8所示为不同薄膜在400~800 nm波段的平均反射率,可以看到,在经过不同能量密度的激光刻蚀处理后,Ag/FTO/AZO多层薄膜的反射率呈现先减小后增大的趋势,这主要取决于两个方面的综合作用:一方面,能量密度增大时,薄膜表面刻蚀光栅结构的高度不断增大,入射光在光栅内表面经多次反射透过薄膜后,有更大的可能在相邻光栅凸起的外表面再次反射,使得部分光重新进入光栅,从而造成散射和吸收损耗<sup>[21]</sup>;另一方面,随着光栅结构高度的不断增大,有利于入射光进行多次反射的光栅总侧面面积不断增大,因此薄膜的抗反射能力不断提高。可以推测:在能量密度从0.1 J/cm<sup>2</sup>增加到0.7 J/cm<sup>2</sup>的过程中,薄膜反射率的下降是光栅总侧面面积增大占主导作用的结果;而在能量密度从0.7 J/cm<sup>2</sup>增加到2.1 J/cm<sup>2</sup>的过程中,薄膜反射率升高则是因为光栅结构的高度过大,造成了较强的光散射和吸收损耗。

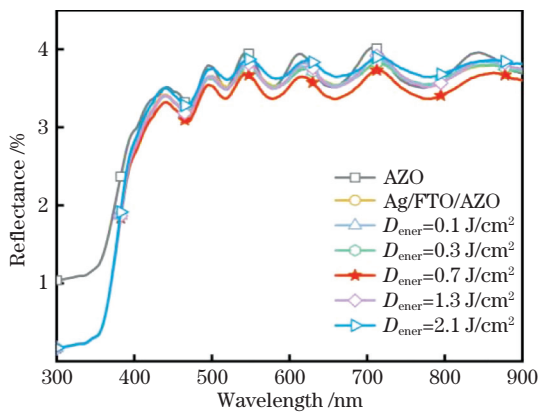


图7 不同薄膜的反射光谱

Fig. 7 Reflectance spectra of different films

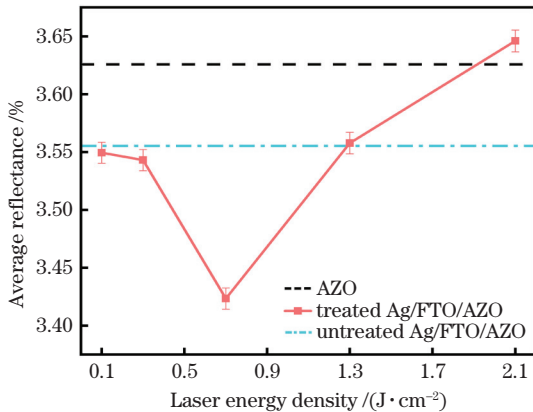


图8 不同薄膜的平均反射率(400~800 nm)

Fig. 8 Average reflectances (400~800 nm) of different films

### 3.4 电学性能分析

图9所示为不同薄膜的方块电阻。原始AZO薄膜的方块电阻为10.5 Ω/sq,未处理的Ag/FTO/AZO

AZO多层薄膜的方块电阻为9.8 Ω/sq,其主要原因是金属Ag层有利于电子传导,从而有效提高了薄膜的导电性<sup>[31]</sup>。当以0.1 J/cm<sup>2</sup>和0.3 J/cm<sup>2</sup>的能量密度在薄膜表面刻蚀光栅结构时,薄膜的方块电阻高于未处理的Ag/FTO/AZO多层薄膜的方块电阻,但是低于原始AZO薄膜的方块电阻,这是因为激光刻蚀光栅结构去除了部分的Ag层和FTO层,降低了薄膜对电子的传导能力,且此时附加激光退火作用不是很强,因此薄膜的方块电阻增大。当激光能量密度从0.1 J/cm<sup>2</sup>增大到0.7 J/cm<sup>2</sup>时,薄膜的方块电阻不断减小,且在0.7 J/cm<sup>2</sup>处达到了最小值,可能是因为此时激光刻蚀产生的附加退火作用是主导因素,虽然去除了部分Ag层和FTO层,导致方块电阻增大,但是退火作用使晶粒尺寸变大,进而减少晶界载流子的散射损失,并提高载流子迁移率,使方块电阻在总体上呈现降低的趋势。而当激光能量密度继续增加到1.3 J/cm<sup>2</sup>和2.1 J/cm<sup>2</sup>时,薄膜的方块电阻增大。结合前面的分析可知,此时单位面积上的热量过大,造成了晶格的无序性增强,降低了载流子的迁移率,同时更多的Ag层和FTO层被去除,两者共同作用下方块电阻变大;再加上能量密度为2.1 J/cm<sup>2</sup>时,激光刻蚀到了玻璃基底,破坏了部分薄膜结构,导致薄膜的方块电阻甚至比原始AZO薄膜的方块电阻还要大。

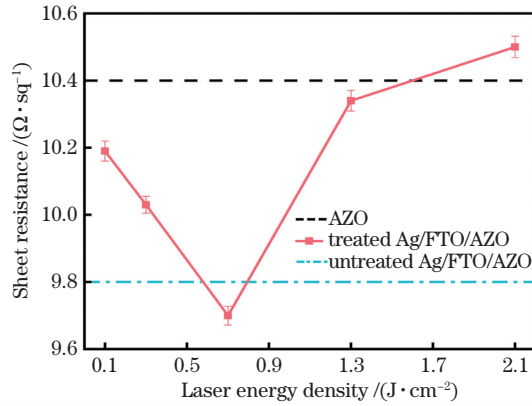


图9 不同薄膜的方块电阻

Fig. 9 Sheet resistances of different films

### 3.5 品质因子

通常情况下,为了评估和比较不同薄膜样品的光学性能和电学性能,需要一个综合的评定标准,而品质因子( $F_{TC}$ )就是这个评定标准。用于计算 $F_{TC}$ 的Haacke方程式为<sup>[32]</sup>

$$F_{TC} = T_{av}^{10}/R_{sh}, \quad (1)$$

式中: $T_{av}$ 为薄膜在400~800 nm波段的平均透过率; $R_{sh}$ 为薄膜的方块电阻。图10所示为不同薄膜

品质因子的变化曲线。可以发现,原始AZO薄膜的品质因子为 $2.58 \times 10^{-2} \Omega^{-1}$ ,与之相比,大部分被激光刻蚀过的Ag/FTO/AZO多层薄膜虽然具有相对较小的方块电阻,但FTO层和Ag层的加入导致薄膜的平均透过率明显降低,因此品质因子也有所下降。当能量密度为 $0.7 \text{ J/cm}^2$ 时,得到的Ag/FTO/AZO多层薄膜的品质因子最大,为 $2.80 \times 10^{-2} \Omega^{-1}$ ,高于原始AZO薄膜的品质因子,表明其综合性能最好。

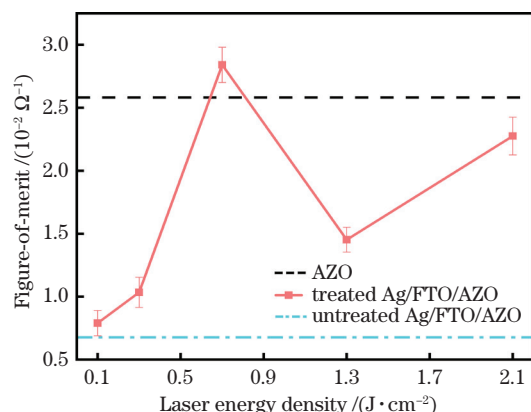


图 10 不同薄膜的品质因子

Fig. 10 Figure-of-merits of different films

## 4 结 论

利用波长为532 nm的纳秒脉冲激光对由磁控溅射法制备的Ag/FTO/AZO多层薄膜进行激光刻蚀来制备光栅结构,研究了经过不同能量密度刻蚀后薄膜的表面形貌、光学性能和电学性能的变化。结果表明,在能量密度为 $0.7 \text{ J/cm}^2$ 的条件下,激光刻蚀产生的光栅结构具有适宜的高度和总侧面面积,能够有效提高薄膜的抗反射能力,同时产生的附加激光退火作用促进了薄膜中晶粒的生长,减少了晶体缺陷数量,使光和载流子的散射损失减少,载流子迁移率提高,最终提高了薄膜的透过率,优化了薄膜的导电性能。本研究中激光刻蚀光栅结构和附加激光退火作用相结合的策略可为透明导电薄膜的性能优化提供有效途径。

## 参 考 文 献

- [1] Seawsakul K, Horprathum M, Eiamchai P, et al. Glancing-angle pulsed dc magnetron sputtered AZO thin films for TCO applications[J]. Materials Today: Proceedings, 2018, 5(6): 14166-14171.
- [2] Sakthivel P, Asaithambi S, Karappaiah M, et al. Improved optoelectronic properties of Gd doped cadmium oxide thin films through optimized film thickness for alternative TCO applications[J]. Journal of Alloys and Compounds, 2020, 820: 153188.
- [3] Leem J W, Song Y M, Lee Y T, et al. Antireflective properties of AZO subwavelength gratings patterned by holographic lithography[J]. Applied Physics B, 2010, 99(4): 695-700.
- [4] Deng Z Y, Jia Q, Feng B, et al. Research progress on fabrication and applications of high-performance films by pulsed laser deposition[J]. Chinese Journal of Lasers, 2021, 48(8): 0802010. 邓钟炀, 贾强, 冯斌, 等. 脉冲激光沉积高性能薄膜制备及其应用研究进展[J]. 中国激光, 2021, 48(8): 0802010.
- [5] Li M L, Liu L, Shen Y. Effect of Ag layer thickness on properties of AZO/Ag/AZO transparent conductive films[J]. Vacuum, 2020, 57(1): 31-34. 李明亮, 刘利, 沈燕. Ag 层厚度对 AZO/Ag/AZO 透明导电薄膜性能的影响[J]. 真空, 2020, 57(1): 31-34.
- [6] Yu J Y, Gao Y, Wang L K, et al. Anti-reductive properties of AZO/FTO bilayered transparent conducting films[J]. Surface Engineering, 2020, 36(1): 1-5.
- [7] Ren N F, Wang W Z, Li B J, et al. Preparation and property optimization of silver-embedded FTO transparent conductive thin films by laser etching and coating AZO layer[J]. Journal of Materials Science: Materials in Electronics, 2021, 32(8): 10644-10661.
- [8] Mutitu J G, Shi S Y, Chen C H, et al. Thin film solar cell design based on photonic crystal and diffractive grating structures[J]. Optics Express, 2008, 16(19): 15238-15248.
- [9] Wang T Y, Bian J T, Li X, et al. Effect of laser induced periodic surface structures on infrared emission characteristics of copper films[J]. Chinese Journal of Lasers, 2021, 48(4): 0401017. 王田宇, 卞进田, 李欣, 等. 激光诱导表面周期性结构对铜薄膜红外发射特性的改变[J]. 中国激光, 2021, 48(4): 0401017.
- [10] Ren N F, Huang L J, Li B J, et al. Laser-assisted preparation and photoelectric properties of grating-structured Pt/FTO thin films[J]. Applied Surface Science, 2014, 314: 208-214.
- [11] Yang H, Huang S, Duan J, et al. Contrastive study on laser ablation of single-crystal silicon by 1030 nm femtosecond laser and 355 nm nanosecond laser[J]. Chinese Journal of Lasers, 2013, 40(1): 0103003. 杨煥, 黄珊, 段军, 等. 飞秒与纳秒激光刻蚀单晶硅对比研究[J]. 中国激光, 2013, 40(1): 0103003.
- [12] Zhang C, Zhang Q M, Guo L, et al. Ablating process with 355 nm laser for amorphous silicon thin-

- film solar cell [J]. High Power Laser and Particle Beams, 2012, 24(11): 2751-2756.
- 张超, 张庆茂, 郭亮, 等. 非晶硅薄膜太阳能电池的紫外激光刻蚀工艺 [J]. 强激光与粒子束, 2012, 24(11): 2751-2756.
- [13] Shang K W, Wu G, Liu X L, et al. Femtosecond laser etching of aluminum film on Tedlar composite surfaces [J]. Chinese Journal of Lasers, 2021, 48(10): 1002117.
- 尚凯文, 吴敢, 刘孝丽, 等. Tedlar复合材料表面飞秒激光刻蚀铝薄膜技术研究 [J]. 中国激光, 2021, 48(10): 1002117.
- [14] Mendes P M, Jacke S, Critchley K, et al. Gold nanoparticle patterning of silicon wafers using chemical e-beam lithography [J]. Langmuir, 2004, 20(9): 3766-3768.
- [15] Takino H, Shibata N, Itoh H, et al. Computer numerically controlled plasma chemical vaporization machining with a pipe electrode for optical fabrication [J]. Applied Optics, 1998, 37(22): 5198-5210.
- [16] Lang T T, Lin X F, He J J. Fabrication of silica-on-silicon arrayed waveguide gratings [J]. Acta Optica Sinica, 2011, 31(2): 0213003.
- 郎婷婷, 林旭峰, 何建军. 硅基二氧化硅阵列波导光栅制作工艺的研究 [J]. 光学学报, 2011, 31(2): 0213003.
- [17] Yi P, Wu Y, Liu N, et al. Intrusion detection for wireless mesh networks using finite state machine [J]. China Communications, 2010, 7(5): 40-48.
- [18] Chou S Y, Krauss P R, Renstrom P J. Imprint of sub-25 nm vias and trenches in polymers [J]. Applied Physics Letters, 1995, 67(21): 3114-3116.
- [19] Yamada R, Nomura N, Saida J J, et al. Fabrication of optical gratings through surface patterning of zirconium-based metallic glass by laser irradiation [J]. Intermetallics, 2018, 93: 377-382.
- [20] Canteli D, Torres I, Fernández S, et al. Photon-collection improvement from laser-textured AZO front-contact in thin-film solar cells [J]. Applied Surface Science, 2019, 463: 775-780.
- [21] Huang L J, Zhao L, Li B J, et al. Improving optical and electrical performances of aluminum-doped zinc oxide thin films with laser-etched grating structures [J]. Ceramics International, 2021, 47(6): 7994-8003.
- [22] Huang L J, Li B J, Ren N F. Enhancing optical and electrical properties of Al-doped ZnO coated polyethylene terephthalate substrates by laser annealing using overlap rate controlling strategy [J]. Ceramics International, 2016, 42(6): 7246-7252.
- [23] Cho J S, Baek S H, Park S H, et al. Effect of nanotextured back reflectors on light trapping in flexible silicon thin-film solar cells [J]. Solar Energy Materials and Solar Cells, 2012, 102: 50-57.
- [24] Tseng S F, Hsiao W T, Huang K C, et al. The effect of laser patterning parameters on fluorine-doped tin oxide films deposited on glass substrates [J]. Applied Surface Science, 2011, 257(21): 8813-8819.
- [25] Berger J, Roch T, Correia S, et al. Controlling the optical performance of transparent conducting oxides using direct laser interference patterning [J]. Thin Solid Films, 2016, 612: 342-349.
- [26] Huang L J, Zhang G M, Li H, et al. Selective laser ablation and patterning on Ag thin films with width and depth control [J]. Journal of Materials Science, 2020, 31(6): 4943-4955.
- [27] Lin T C, Huang W C, Tsai F C. Hydrogen plasma effect toward the AZO/CuCr/AZO transparent conductive electrode [J]. Microelectronic Engineering, 2017, 167: 85-89.
- [28] Pillai S, Catchpole K R, Trupke T, et al. Surface plasmon enhanced silicon solar cells [J]. Journal of Applied Physics, 2007, 101(9): 093105.
- [29] Ren N F, Zu W, Li B J, et al. Research on laser irradiation treatment and photoelectric property of Ti/FTO composite films [J]. Chinese Journal of Lasers, 2017, 44(5): 0502004.
- 任乃飞, 祖伟, 李保家, 等. Ti/FTO 复合薄膜的激光辐照处理及其光电性能研究 [J]. 中国激光, 2017, 44(5): 0502004.
- [30] Hezam M, Tabet N, Mekki A. Synthesis and characterization of DC magnetron sputtered ZnO thin films under high working pressures [J]. Thin Solid Films, 2010, 518(24): e161-e164.
- [31] Guo K, Yu T, Song B B, et al. Fabrication and optoelectronic properties of ZnO/Ag/ZnO composite films at room temperature [J]. Laser & Optoelectronics Progress, 2017, 54(10): 103102.
- 郭凯, 于涛, 宋斌斌, 等. 常温下 ZnO/Ag/ZnO 复合薄膜的制备及其光电特性 [J]. 激光与光电子学进展, 2017, 54(10): 103102.
- [32] Demirhan Y, Koseoglu H, Turkoglu F, et al. The controllable deposition of large area roll-to-roll sputtered ITO thin films for photovoltaic applications [J]. Renewable Energy, 2020, 146: 1549-1559.

# Influences of Laser Etching on Optical and Electrical Properties of Ag/FTO/AZO Thin Films

Zhou Yunlong<sup>1</sup>, Lei Min<sup>1</sup>, Wang Chenlin<sup>1</sup>, Xu Qian<sup>1</sup>, Li Baojia<sup>1,2\*</sup>, Huang Lijing<sup>2,3\*\*</sup>

<sup>1</sup> School of Material Science and Engineering, Jiangsu University, Zhenjiang, Jiangsu 212013, China;

<sup>2</sup> Institute of Micro-nano Optoelectronic and Terahertz Technology, Jiangsu University, Zhenjiang, Jiangsu 212013, China;

<sup>3</sup> School of Mechanical Engineering, Jiangsu University, Zhenjiang, Jiangsu 212013, China

## Abstract

**Objective** In the application field of photoelectric devices, such as solar cells and liquid crystal displays, researchers pay attention to the aluminum-doped zinc oxide (AZO) film due to its abundant raw materials, high stability, low cost, and non-toxicity. An Ag layer is typically deposited on the surface of an AZO film to improve its electrical conductivity; however, the addition of the Ag layer inevitably results in the film's light reflection loss, which leads to a decrease in its optical transmittance. Although the light reflection in the AZO film can be inhibited to a certain extent using a fluorine-doped tin oxide (FTO) composite layer between the Ag layer and AZO film, its inhibition is limited, and a very-large thickness of the FTO layer will also lead to the decrease in optical transmittance of the film. Grating structures fabricated on film surfaces have been confirmed to have anti-reflection effects, and the laser etching method used for grating structure fabrication has advantages such as high efficiency, easy operating, and controllability. Hence, laser etching of grating structures on Ag/FTO/AZO multilayer film surfaces was performed in this study. It has been demonstrated that the anti-reflection effects of laser-etched grating structures can effectively improve the optical transmittance of the films and that the optical transparency and electrical conductivity of the films can be improved further by the additional laser annealing effect during laser etching. This study is expected to provide a simple and effective method for optimizing the performance of single-layer or multilayer films, as well as a scientific foundation for the application of laser-etched grating structures.

**Methods** Ag/FTO/AZO multilayer films were prepared by radio frequency magnetron sputtering with commercial AZO films as the substrates. The as-obtained Ag/FTO/AZO films were then placed on the movable sample stage of a diode pumped Nd:YVO<sub>4</sub> nanosecond-pulsed laser system ( $\lambda = 532$  nm) and laser-etched with different laser energy densities to fabricate grating structures. The effects of laser energy density on surface morphology, crystal structure, optical properties, and electrical properties of films were studied. The surface morphologies of the films after laser etching were observed by scanning electron microscope. The heights of the grating structures were determined by a confocal laser scanning microscope. An X-ray diffractometer was used to determine the crystal structures of the films. A UV-visible spectrophotometer was used to measure the optical transmittance and reflectance of the film samples (Shanghai Metash Instruments: UV-8000). A digital four-point probe instrument was used to measure the sheet resistance values of the film samples (Guangzhou 4-PROBES TECH: RTS-9).

**Results and Discussions** The results showed that with the increase in laser energy density, the melting area of the Ag/FTO/AZO film surfaces extended to the low-temperature zone driven by the Marangoni convection, temperature difference, and pressure difference, which caused increases in width and depth of the laser-etched grooves, as well as in the total lateral area of the grating structures on the film surfaces (Figs. 2 and 3). With increasing laser energy density, the additional laser annealing effect during laser etching was gradually strengthened. When the laser energy density was increased from  $0.1 \text{ J/cm}^2$  to  $0.7 \text{ J/cm}^2$ , the total lateral area of the grating structure increased, and the light reflection loss on the grating's outer surface was avoided (Figs. 7 and 8). The increased width of the laser-etched grooves increased the area of the film that was thinning. Furthermore, the reinforced additional laser annealing effect promoted grain growth and decreased crystal defects in the film to improve crystallinity (Fig. 4), thus reducing light scattering loss in the film. These three factors increased the optical transmittance of the film (Figs. 5 and 6). The additional laser annealing effect, on the contrary, reduced the carrier scattering loss at grain boundaries and increased carrier mobility, lowering the sheet resistance of the film (Fig. 9). The height of the laser-etched grating structure increased as the laser energy density increased from  $0.7 \text{ J/cm}^2$  to  $2.1 \text{ J/cm}^2$ , resulting in more light scattering and absorption losses caused by the reflection of the

incident light on the grating's outer surface, thus leading to an increase in optical reflectance of the film. When the laser energy density was  $2.1 \text{ J/cm}^2$ , the laser etching depth (i.e. the height of the laser-etched grating structure) was too large and even reached the glass substrate. Therefore, the optical transmittance of the film decreased at first and then increased. The excessive laser energy density ( $1.3 \text{ J/cm}^2$  and  $2.1 \text{ J/cm}^2$ ) caused lattice disorder in the film and the removal of more Ag and FTO layer materials, thereby reducing the film's electrical conductivity. The optical transmittance and sheet resistances of the films were used to calculate the figure-of-merits used to evaluate the film's comprehensive properties. The calculation results showed that its variation trend rose at first, then decreased, and then rose again (Fig. 10).

**Conclusions** In this study, laser etching using a laser energy density of  $0.7 \text{ J/cm}^2$  resulted in a grating structure with an appropriate height and total side area on the Ag/FTO/AZO film surface, which could effectively improve the anti-reflection ability of the film. Furthermore, the additional laser annealing effect produced during laser etching promoted grain growth in the film, reduced crystal defects, and resulted in less light and carrier scattering loss and higher carrier mobility. Therefore, the film's optical transmittance and electrical conductivity were enhanced. The resulting film received the highest figure-of-merit ( $2.80 \times 10^{-2} \Omega^{-1}$ ), indicating that its overall quality was superior to that of the original AZO film ( $2.58 \times 10^{-2} \Omega^{-1}$ ).

**Key words** laser processing; Ag/FTO/AZO film; grating structure; optical property; electrical property